Topological approach to baryon-antibaryon and meson production in rapidly expanding Bjorken rods

G. Holzwarth*
Siegen University, 57068 Siegen, Germany
(Received 26 April 2004; published 9 August 2004)

The topological approach to baryon-antibaryon production in the chiral phase transition is numerically simulated for rapidly expanding hadronic systems. For that purpose the dynamics of the effective chiral field is implemented on a space-rapidity lattice. The essential features of evolutions from initial ''hot'' configurations into final ensembles of (anti-)baryons embedded in the chiral condensate are studied in proper time of comoving frames. Typical times for onset and completion of the roll-down and exponents for the growth of correlations are extracted. Meson and baryon-antibaryon yields are estimated. For standard assumptions about initial coherence lengths they are compatible with experimental results.

DOI: 10.1103/PhysRevD.70.036001 PACS number(s): 11.10.Lm, 11.27.+d, 25.75.−q, 64.60.Cn

I. INTRODUCTION

The topological approach to baryon structure and dynamics in the framework of an effective action for mesonic chiral fields has achieved a number of remarkable successes. The soliton concept [1] for baryons provides an impressive account of spectrum and properties of baryon resonances (essentially without numerous ''missing resonances'') [2], with predictive power that recently has even led to the first indications for pentaquarks [3]. Model-independent relations between T-matrix elements for meson-baryon scattering [4] and explicit results for specific channels are well supported by experimental data [5]. The matrix element of the axial singlet current related to the spin content of the proton is naturally of the observed order of magnitude [6]. The ''unexpected'' behavior recently found [7] in the ratio of electric and magnetic proton form factors has been predicted in this approach long ago [8]. The underlying chiral effective action is profoundly based on the $1/N_c$ expansion of QCD [9], preserving all relevant symmetries. Efforts to include next-to-leading order quantum corrections have brought substantial improvement as expected [10].

The manifestations of a chiral phase transition pose another natural challenge for an effective theory with a ground state that is characterized by spontaneously broken symmetry. The possible formation of disoriented domains [11] during the growth of the chiral condensate has been in the focus of interest for some time. But signatures in terms of anomalous multiplicity ratios for differently charged pions have not been observed [12], in accordance with theoretical conclusions [13,14]. Anomalies in antibaryon production were very early recognized as possible signals for interesting dynamics [15] in that phase transition, and the concept to consider baryons as topological solitons in a chiral condensate should lead to quite definite expectations for this process.

Meanwhile, in relativistic heavy-ion collisions at RHIC, very high energy densities are being produced in extended spatial regions that are essentially baryon free and well separated in rapidity from the nuclear slabs receding from the collision volume. The experimental values found in the central rapidity region for the ratio of the integrated $\bar{p}$ to π^- yields lies between 0.065 and 0.075 [16]. This is still too close to the thermal equilibrium $\bar{p}/\pi^-$ ratio (for a typical plasma temperature of $\mathcal{T}\sim 200$ MeV),

$$\bar{p}/\pi^- \sim 2\exp[(m_\pi - m_p)/\mathcal{T}] = 0.035, \tag{1}$$

to constitute a clear indication for interesting underlying physics. Still, although the experimental result does not look very exciting, it still poses a constraint for the possible validity of the soliton concept, because any conceivable dynamical production process must be able to produce a comparable number.

In the topological approach the number of baryon-antibaryon pairs produced during the chiral phase transition depends on two factors: the first is the modulus $|\rho|$ of the average winding density present in the initial ''hot'' field configuration. In analogy to applications in cosmology [17] and condensed matter systems [18] this quantity is closely related to the coherence length for the local orientations of the chiral field $\mathbf{\Phi}$. Without detailed knowledge about the initial field configurations this coherence length enters as a parameter and takes away stringent predictive power from the approach. However, different conjectures about the nature of the initial field ensemble suggest typical ranges for the coherence lengths that then may be discriminated by the experimentally observed abundancies.

The second factor is the reduction of the initially present total $n_i = \int |\rho| dV$ through the dynamical ordering process, which finally leads to the formation of stable soliton structures embedded in the topologically trivial ordered chiral condensate of the ''cold'' system. The solitons or antisolitons evolve from topological obstacles that are met by the aligning field orientations, and develop into their stable ''cold'' form during the course of the evolution. At the end, the same integral $n_f = \int |\rho| dV$ counts the number of finally surviving nontrivial separate structures, so it is identified with the number of baryons and antibaryons created in the process. The decrease of n during the roll-down is reasonably well repre-

*Email address: holzwarth@physik.uni-siegen.de

sented by a power law $(\tau/\tau_0)^{-\gamma}$ and the exponent γ can be measured in numerical simulations. Evidently, the initial time τ_0 that marks the onset of the evolution enters here as a second parameter which further reduces the predictive power of the approach. Fortunately, it turns out that γ is rather small, so the dependence on τ_0 is only weak.

Measuring γ and the time τ_f when the roll-down is completed presents a typical task for numerical simulations once the equation of motion (EOM) that governs the field evolutions is implemented on a lattice. The underlying effectice chiral action is known from other applications, so no additional parameters enter at this point. In condensed matter applications, a phase transition is generally driven by an externally imposed quench, or by a dissipative term included in the EOM. In cosmology or in our present heavy-ion application it is the rapid expansion of the hot volume that drives the cooling process. This expansion is efficiently implemented [19] by transforming to rapidity–proper-time coordinates, i.e., by boosting to the local comoving frame. This is especially convenient if we consider a system that expands only in one (longitudinal) direction with its transverse scales unchanged (the Bjorken rod). The resulting dilution of the longitudinal gradients drives the system towards its global minimum. However, as there is no genuine dissipation in the system, the total energy approaches a constant that resides in the chiral fluctuations around the global minimum. Thus, the simulations also allow us to estimate π- or σ- meson abundancies.

Naturally, before the field configurations can roll down towards the global minimum, the potential $V(\Phi^2,\mathcal{T})$ that underlies the EOM must have changed from the ''hot'' chirally symmetric form to its ''cold'' symmetry-violating form. But, during the early stages, the evolutions are dominated by local aligning of the field orientation $\hat{\mathbf{\Phi}}$. During this phase the form of the potential is not important. So its time dependence can be replaced by a sudden quench where the ''hot'' field configuration is exposed to the ''cold'' potential $V(\Phi^2,\mathcal{T}=0)$, from the outset at initial time τ_0. In the following, for definiteness we make use of this sudden quench approximation (although the simulations, of course, allow us to study other cases as well).

For the sake of simplicity we first discuss all relevant features for the case of the two-dimensional O(3) model, with only one spatial dimension transverse to the longitudinal rapidity coordinate. Except for computational complexity the extension to the three-dimensional O(4) field presents no essential new features. The effective action, its transformation to the Bjorken frame, and the resulting EOM are presented in Sec. II. It is important for the choice of the initial ensemble of field configurations that it allows us in a convenient way to monitor the initial coherence lengths because they are the crucial parameters for the final baryon-antibaryon multiplicities. We choose an isotropic Gaussian random ensemble of field fluctuations in momentum space that is characterized by a temperaturelike parameter to be able to compare with other approaches. Of course, this is not necessary. In fact, even at initial time τ_0 the longitudinally expanding Bjorken rod need not be an isotropic system, and it may be physically justified to distinguish already in the initial ensemble two different longitudinal and transverse correlation lengths. This is easy to incorporate, but in Sec. III we present initial conditions that are locally isotropic.

As discussed elsewhere [20] stable solitons shrink in a spatially expanding frame. Therefore, lattice implementations of their dynamics will necessarily involve lattice artifacts after some time. These are discussed in Sec. IV. They can be isolated and subtracted from the physically interesting quantities.

In Sec. V the essential features of typical evolutions are discussed. Estimates for the times of onset and completion of the roll-down are obtained, and the dynamical exponents for the growth of correlation lengths and decrease of defect number are established and compared. The spectrum of the fluctuations remaining after the roll-down is considered and finally the mesonic and baryonic multiplicities are obtained.

The extension to the physically interesting (3+1)-dimensional O(4) field is discussed in Sec. VI. The topological generalization is well known, the additional transverse dimension is of little influence for the growth exponents. However, the coupling constants in the effective action here are related to physical quantities, so they are known (except for some uncertainty concerning the σ mass), and the results can be compared with experimentally determined abundance ratios.

Of course, it would be desirable to obtain a very definite answer whether the topological approach to antibaryon production in a chiral phase transition is validated or ruled out by the data. However, with our poor knowledge about the initial conditions in the hot plasma after a heavy-ion collision, we cannot expect much more than allowed ranges for the relevant parameters, which hopefully overlap with standard ideas about coherence lengths and formation times.

II. THE EFFECTIVE ACTION IN THE BJORKEN FRAME

For simplicity we first discuss the (2+1)-dimensional O(3) model. It is defined in terms of the dimensionless 3-component field $\mathbf{\Phi}=\Phi\hat{\mathbf{\Phi}}$ with unit-vector field $\hat{\mathbf{\Phi}}$ ($\hat{\mathbf{\Phi}}\cdot\hat{\mathbf{\Phi}}=1$), and modulus (bag) field Φ, with the following Lagrangian density in 2+1 dimensions (x,z,t)

$$\mathcal{L}=f_\pi^2(\mathcal{L}^{(2)}+\mathcal{L}^{(4)}+\mathcal{L}^{(0)}) \tag{2}$$

(f_π^2 is an overall constant of dimension [mass^1], so the physical fields $f_\pi\mathbf{\Phi}$ are of mass dimension [mass$^{1/2}$]). The second-order part $\mathcal{L}^{(2)}$ comprises the kinetic terms of the linear σ model

$$\mathcal{L}^{(2)}=\frac{1}{2}\partial_\mu\mathbf{\Phi}\partial^\mu\mathbf{\Phi}, \tag{3}$$

$\mathcal{L}^{(4)}$ is the four-derivative ''Skyrme'' term (which involves only the unit-vector field $\hat{\mathbf{\Phi}}$) defined in terms of the topological current ρ_μ

$$\rho^\mu=\frac{1}{8\pi}\epsilon^{\mu\nu\rho}\hat{\mathbf{\Phi}}\cdot(\partial_\nu\hat{\mathbf{\Phi}}\times\partial_\rho\hat{\mathbf{\Phi}}) \tag{4}$$

(which satisfies $\partial_\mu \rho^\mu = 0$),

$$\mathcal{L}^{(4)} = -\lambda \ell^2 \varrho_\mu \varrho^\mu = -\frac{2\lambda \ell^2}{(8\pi)^2}[(\partial_\mu \hat{\mathbf{\Phi}} \partial^\mu \hat{\mathbf{\Phi}})^2 - (\partial_\mu \hat{\mathbf{\Phi}} \partial_\nu \hat{\mathbf{\Phi}}) \times (\partial^\mu \hat{\mathbf{\Phi}} \partial^\nu \hat{\mathbf{\Phi}})], \tag{5}$$

and $\mathcal{L}^{(0)}$ contains the Φ^4 potential and an explicit symmetry-breaker in the three-direction

$$\mathcal{L}^{(0)} = -V(\mathbf{\Phi}, \mathcal{T}) = -\frac{1}{\ell^2}\left(\frac{\lambda}{4}[\mathbf{\Phi}^2 - f(\mathcal{T})^2]^2 - H\Phi_3\right) - \text{const} \tag{6}$$

with dimensionless coupling constants λ and H, and

$$f^2(\mathcal{T}) = f_0^2(\mathcal{T}) - \frac{H}{\lambda f_0(\mathcal{T})}. \tag{7}$$

This choice ensures that the global minimum of the potential $V(\mathbf{\Phi}, \mathcal{T})$ is always located at $\mathbf{\Phi}_0 = (0,0,f_0(\mathcal{T}))$. Generically, the function $f_0^2(\mathcal{T})$ decreases from $f_0^2 = 1$ at $\mathcal{T} = 0$ towards zero for large $\mathcal{T}$. The constant in the potential (6) is chosen such that the value of the potential V at $\mathbf{\Phi} = 0$ is independent of $\mathcal{T}$[given by the constant $V(0,\mathcal{T}) = (\lambda + 2H)/(4\ell^2)$], and at the $\mathcal{T} = 0$ minimum $\mathbf{\Phi} = \mathbf{\Phi}_0 = (0,0,1)$ we have $V(\mathbf{\Phi}_0, \mathcal{T} = 0) = 0$.

The masses of the π and σ fluctuations $(\pi_1, \pi_2, f_0 + \sigma)$ around this minimum are

$$m_\pi^2 = \frac{H}{\ell^2 f_0}, \quad m_\sigma^2 = \frac{2\lambda f_0^2}{\ell^2} + m_\pi^2. \tag{8}$$

Without explicit symmetry breaking, $H = 0$, we assume that $f^2(\mathcal{T})$ changes sign at $\mathcal{T} = \mathcal{T}_c$, such that $\mathbf{\Phi}_0 = (0,0,0)$ and $m_\sigma^2 = m_\pi^2 = m^2 = \lambda |f^2| / \ell^2$ for $\mathcal{T} > \mathcal{T}_c$.

The parameter ℓ (with dimension of a length) that we have separated out from the coupling constants of potential and Skyrme terms can be absorbed into the spatial coordinates $\boldsymbol{x}$. So it characterizes the spatial radius of stable extended solutions (which scales like $1/\sqrt{f^2}$). As ℓ simply sets the spatial scale, it could be put equal to one, as long as no other (physical or artificial) length scales are relevant. For lattice implementations, however, the lattice constant a and the size of the lattice (Na) set (usually unphysical) scales. To avoid artificial scaling violations we have to ensure that the size of physical structures (like solitons) is large as compared to the lattice constant a and small as compared to the lattice size Na. So, for numerical simulations we have to choose $1 \ll \ell/a \ll N$. It has been shown in Ref. [21] that for solitons that extend over more than at least 4–5 lattice units the energy E_B is independent of ℓ/a. So, in the following we will adopt $\ell/a \sim 5$ as sufficiently large. This appears also as physically reasonable, if we consider typical lattice constants of 0.2 fm and baryon radii of about 1 fm. On the other hand this will require lattice sizes of at least $N \sim 50$ to avoid boundary effects for the structure of individual solitons. Unfortunately, in the Bjorken frame that we shall use in the following, the longitudinal extension of stable solitons shrinks like τ^{-1} as function of proper time τ. This means that after times of order ℓ the simulations will be influenced by lattice artifacts, which may even dominate for large times.

For rapid expansion in the (longitudinal) z direction we perform the transformation from (z,t) to locally comoving frames (η, τ) with proper time τ and rapidity η, defined through

$$t = \tau \cosh\eta, \quad \tau = \sqrt{t^2 - z^2}, \quad \partial_t = \cosh\eta \, \partial_\tau - \frac{\sinh\eta}{\tau}\partial_\eta,$$

$$z = \tau \sinh\eta, \quad \eta = \operatorname{atanh}\left(\frac{z}{t}\right),$$

$$\partial_z = -\sinh\eta \, \partial_\tau + \frac{\cosh\eta}{\tau}\partial_\eta. \tag{9}$$

Inserting (9) into (3) and (5) leaves the form of $\mathcal{L}^{(2)}$ and $\mathcal{L}^{(4)}$ invariant, with ∂_t replaced by ∂_τ, and ∂_z replaced by $(1/\tau)\partial_\eta$. The specific structure of the Skyrme term again eliminates all terms with four τ or η derivatives. For the effective action we take the integration boundaries from $-\infty$ to $+\infty$ for rapidity η and for the transverse coordinate x. The three-dimensional space-time volume element $dxdzdt$ is replaced by $\tau dx d\eta d\tau$. Therefore, in a separation of the action $\mathcal{S}$ in kinetic terms T, gradient terms L, and the potential U,

$$\mathcal{S} = \int d\tau \int_{-\infty}^{+\infty} \mathcal{L} d\eta dx = \int (T_\perp + T_\parallel - L_\perp - L_\parallel - U) d\tau \tag{10}$$

the longitudinal $\parallel$ terms involving rapidity gradients carry a factor $1/\tau$, while all other terms carry a factor τ. So we have

$$T_\perp = \tau \int \left\{ \frac{1}{2}(\partial_\tau \mathbf{\Phi} \partial_\tau \mathbf{\Phi}) + \frac{\lambda \ell^2}{(4\pi)^2}\left[\frac{\mathbf{\Phi}}{\Phi^3} \cdot (\partial_\tau \mathbf{\Phi} \times \partial_x \mathbf{\Phi})\right]^2 \right\} \times d\eta dx, \tag{11}$$

$$T_\parallel = \frac{1}{\tau} \int \left\{ \frac{\lambda \ell^2}{(4\pi)^2}\left[\frac{\mathbf{\Phi}}{\Phi^3} \cdot (\partial_\tau \mathbf{\Phi} \times \partial_\eta \mathbf{\Phi})\right]^2 \right\} d\eta dx, \tag{12}$$

$$L_\perp = \tau \int \left\{ \frac{1}{2}(\partial_x \mathbf{\Phi} \partial_x \mathbf{\Phi}) \right\} d\eta dx, \tag{13}$$

$$L_\parallel = \frac{1}{\tau} \int \left\{ \frac{1}{2}(\partial_\eta \mathbf{\Phi} \partial_\eta \mathbf{\Phi}) + \frac{\lambda \ell^2}{(4\pi)^2}\left[\frac{\mathbf{\Phi}}{\Phi^3} \cdot (\partial_\eta \mathbf{\Phi} \times \partial_x \mathbf{\Phi})\right]^2 \right\} \times d\eta dx, \tag{14}$$

$$U = \tau \int \left\{ \frac{\lambda}{4\ell^2}(\mathbf{\Phi}^2 - f^2)^2 - \frac{H}{\ell^2}\Phi_3 + \text{const} \right\} d\eta dx. \tag{15}$$

Variation of $\mathcal{S}$ with respect to $\mathbf{\Phi}$ leads to the equation of motion (EOM).

The contributions of $\mathcal{L}^{(4)}$ to the longitudinal and transverse parts $T_\parallel$ and $T_\perp$ of the kinetic energy cause certain numerical difficulties for the implementation of the EOM on a lattice. They require at every time step the inversion of matrices that depend on gradients of the unit vectors $\hat{\mathbf{\Phi}}$, which multiply first and second time derivatives of the chiral field. This can be troublesome in areas where the unit vectors are aligned, and can be poorly defined in regions where the unit vectors vary almost randomly for next-neighbor lattice points (i.e., for initially random configurations, or near the center of defects). In any case, stabilizing the evolutions requires extremely small time steps and leads to very time-consuming procedures. Although these problems can be handled, we have compared the results with evolutions where the kinetic energy is taken from $\mathcal{L}^{(2)}$ alone. For coupling strengths $\lambda\ell^2$ within reasonable limits, we find that the resulting differences do not justify the large additional expense caused by the fourth-order kinetic contributions. Evidently, the reason is that the EOM determines the field velocities (depending on the functional form of the kinetic energy) in such a way that the numerical value of the total kinetic energy is not very sensitive to its functional form. We therefore use in the following an effective action where the kinetic terms (11) and (12) are replaced by

$$T_\perp = \frac{\tau}{2}\int (\partial_\tau \mathbf{\Phi}\partial_\tau \mathbf{\Phi}) d\eta dx, \quad T_\parallel = 0. \tag{16}$$

With this simplification the EOM is

$$\frac{1}{\tau}\partial_\tau \mathbf{\Phi} + \partial_{\tau\tau}\mathbf{\Phi} - \partial_{xx}\mathbf{\Phi} - \frac{1}{\tau^2}\partial_{\eta\eta}\mathbf{\Phi} + \frac{\lambda}{\ell^2}(\Phi^2 - f^2)\mathbf{\Phi} - \frac{H}{\ell^2}\hat{\boldsymbol{e}}_3 + \frac{\lambda\ell^2}{\tau^2}\frac{\delta\rho_0^2}{\delta\mathbf{\Phi}} = 0. \tag{17}$$

This form has the big advantage that we can make use of the geometrical meaning of the winding density ρ_0 as the area of a spherical triangle, bounded by three geodesics on a two-dimensional spherical surface. In closed form it is expressed through the unit vectors pointing to its corners, and does not involve gradients. So this allows for a very accurate and fast lattice implementation of the last term in the EOM.

III. INITIAL CONFIGURATIONS

We assume that at an initial proper time τ_0 the system consists of a hadronic fireball with energy density ε_0 stored in a random ensemble of hadronic field fluctuations. Subsequently, for $\tau > \tau_0$, it is subject to EOM (17). The initial condition and the symmetry of the action imply boost invariance, i.e., the system looks the same in all locally comoving frames, so it is sufficient to consider its dynamics in a rapidity slice of size $\Delta\eta$ near midrapidity $\eta = 0$, which constitutes a section of the initially created Bjorken rod with transverse extension $\mathcal{A}$. The energy $E = T + L + U$ in this slice then is given by an η integral that extends over the finite rapidity interval $\Delta\eta$ and represents the energy contained in a comoving volume $\mathcal{V} = \tau\Delta\eta\mathcal{A}$. Due to the symmetry of the initial condition this comoving volume grows with increasing proper time τ into spatial regions with high energy density; therefore E contains contributions that increase with τ. The average energy density $\varepsilon = E/\mathcal{V}$ satisfies $d\varepsilon/d\tau \leqslant 0$.

For numerical simulations we implement the configurations $\mathbf{\Phi}(x,\eta,\tau)$ on a rectangular lattice $(x,\eta) = (ia, jb)$ $(i,j = 1,\ldots,N)$ with lattice constants a for the transverse coordinate and b for the rapidity lattice. We define the initial configurations $\mathbf{\Phi}_{ij}$ at the lattice sites (i,j) as Fourier transforms of configurations $\tilde{\mathbf{\Phi}}_{kl}$ on a momentum lattice

$$\mathbf{\Phi}_{ij} = \frac{1}{N}\sum_{k,l=-N/2+1}^{N/2}\frac{1}{2}(e^{\mathrm{i}(2\pi/N)(i\cdot k + j\cdot l)}\tilde{\mathbf{\Phi}}_{kl} + \text{c.c.}), \tag{18}$$

with $\tilde{\mathbf{\Phi}}^*_{kl} = \tilde{\mathbf{\Phi}}_{-k-l}$. Inversely, the real parts $\boldsymbol{\alpha}_{kl}$ and the imaginary parts $\boldsymbol{\beta}_{kl}$ of $\tilde{\mathbf{\Phi}}_{kl}$ are obtained from the real configuration $\mathbf{\Phi}_{ij}$ through

$$\boldsymbol{\alpha}_{kl} = \frac{1}{N}\sum_{i,j=1}^{N}\cos\frac{2\pi}{N}(ik+jl)\mathbf{\Phi}_{ij} = \boldsymbol{\alpha}_{-k-l}, \tag{19}$$

$$\boldsymbol{\beta}_{kl} = -\frac{1}{N}\sum_{i,j=1}^{N}\sin\frac{2\pi}{N}(ik+jl)\mathbf{\Phi}_{ij} = -\boldsymbol{\beta}_{-k-l}, \tag{20}$$

so we obtain the spectral power P_{pq} of the configurations (or a specific component of it) at any time τ from

$$P_{pq} = \tilde{\mathbf{\Phi}}_{kl}\cdot\tilde{\mathbf{\Phi}}^*_{kl} = \boldsymbol{\alpha}_{kl}\cdot\boldsymbol{\alpha}_{kl} + \boldsymbol{\beta}_{kl}\cdot\boldsymbol{\beta}_{kl} \tag{21}$$

for any transverse or longitudinal momentum $(p,q) = (2\pi/aN)(k,l)$, for $k,l = -N/2+1,\ldots,N/2$.

For the initial configurations at $\tau = \tau_0$ the real and imaginary parts of each of the three components of $\tilde{\mathbf{\Phi}}_{kl}$ at each momentum-lattice point (p,q) are chosen randomly from a Gaussian deviate $G_{kl}(\tilde{\Phi})$ with kl-dependent width σ_{kl},

$$G_{kl}(\tilde{\Phi}) = \frac{1}{\sqrt{2\pi\sigma_{kl}^2}}\exp\left(-\frac{\tilde{\Phi}^2}{2\sigma_{kl}^2}\right),$$

with

$$\sigma_{kl}^2 = \frac{\sigma_0^2}{Z}\exp\left(-\frac{\sqrt{p^2+q^2+m^2}}{\mathcal{T}}\right), \tag{22}$$

with normalization Z chosen in such a way that

$$\sum_{k,l=-N/2+1}^{N/2}\sigma_{kl}^2 = N^2\sigma_0^2. \tag{23}$$

[In the continuum limit $(a\to 0,\ N\to\infty)$ we have $Z = (\mathcal{T}^2/2\pi)(1+m/\mathcal{T})e^{-m/\mathcal{T}}$.]

In other words, we choose a Boltzmann distribution for the average occupation numbers $n_{kl} = \langle\langle\tilde{\Phi}_{kl}\tilde{\Phi}^*_{kl}\rangle\rangle = \sigma_{kl}^2$ for

each field component, as for relativistic (noninteracting) particles with mass m. Here the mass m^2 is defined by the absolute value

$$m^2(\mathcal{T}) = \frac{\lambda}{\ell^2}|f^2(\mathcal{T})| \tag{24}$$

for the fluctuations around $\mathbf{\Phi}=\mathbf{0}$ in the symmetric potential (6) at the initially high temperature $\mathcal{T}=\mathcal{T}_0$, where $f^2(\mathcal{T})$ is negative. The amplitude σ_0^2 plays the role of a fugacity

$$\sigma_0^2 = \exp(-\mu/\mathcal{T}) \tag{25}$$

for negative chemical potential μ. In the temperature range that we consider ($0.05<a\mathcal{T}<0.8$) (cf. Fig. 3) a suitable value for μ is $a\mu\sim-0.6$. (With this choice the average amplitude of the chiral field is not subject to abrupt deviations from its initial value immediately after the onset of the dynamical evolution.)

We assume isotropy of the initial ensemble with respect to rotations in O(3) space such that the three components of the field fluctuations $\tilde{\Phi}_{kl}^{\alpha}$ ($\alpha=1,2,3$) have the same average square amplitude σ_{kl}^2. By picking each component independently at each point (k,l) from the Gaussian ensemble, different components are uncorrelated and equal components at different points (on the momentum lattice) are also uncorrelated,

$$\begin{aligned}\langle\langle\tilde{\Phi}_{kl}^{\alpha}\tilde{\Phi}_{k'l'}^{\beta *}\rangle\rangle &= \langle\langle\alpha_{kl}^{\alpha}\alpha_{k'l'}^{\beta}\rangle\rangle + \langle\langle\beta_{kl}^{\alpha}\beta_{k'l'}^{\beta}\rangle\rangle \\ &= \sigma_{kl}^2\delta_{\alpha\beta}\left(\frac{1}{2}(\delta_{kk'}\delta_{ll'}+\delta_{-kk'}\delta_{-ll'})\right. \\ &\quad \left.+\frac{1}{2}(\delta_{kk'}\delta_{ll'}-\delta_{-kk'}\delta_{-ll'})\right) \\ &= \sigma_{kl}^2\delta_{\alpha\beta}\delta_{kk'}\delta_{ll'}.\end{aligned} \tag{26}$$

Together with (18) this leads to the fluctuation in the real field configurations

$$\langle\langle\Phi_{ij}^{\alpha}\Phi_{ij}^{\beta}\rangle\rangle = \delta_{\alpha\beta}\frac{1}{N^2}\sum_{k,l=-N/2+1}^{N/2}\sigma_{kl}^2 = \delta_{\alpha\beta}\sigma_0^2, \tag{27}$$

which is, of course, independent of the lattice point (i,j). Its magnitude is controlled by the constant σ_0^2 in (22). It should be sufficiently small to keep the amplitudes of the average initial fluctuations small. On the lattice the upper limit for the momenta p,q is π/a (i.e., $k,l=N/2$). So, as long as

$$\mathcal{T}\ll\frac{\pi}{a}, \tag{28}$$

the lattice cutoff (upper limit momentum) imposed by the finite lattice constant is unimportant because the corresponding states are almost unoccupied. Note that periodicity and antisymmetry of the imaginary parts in (19) requires that $\boldsymbol{\beta}_{kl}$ vanishes if both k and l are multiples of $N/2$. With the condition (28) satisfied, this holds with good accuracy also for the initial configuration picked randomly from the ensemble (22).

The average number of topological defects in a random ensemble of vector configurations is closely related to the characteristic angular coherence length in that ensemble. Therefore, it will be necessary to measure the (equal-time) correlation functions for the unit-vector fields $\hat{\mathbf{\Phi}}$ for the evolving ensembles. In order to have an analytical result at least for the initial configurations (where length and orientation of the three-vectors are uncorrelated), it is easier to consider the correlations among the full vectors $\mathbf{\Phi}$. Therefore, we define normalized transverse and longitudinal correlation functions

$$\begin{aligned}C_{\perp}(i) &= \frac{1}{3\sigma_0^2N^2}\left[\left\langle\left\langle\sum_{m,n=1}^{N}\mathbf{\Phi}_{mn}\cdot\mathbf{\Phi}_{m+i,n}\right\rangle\right\rangle\right. \\ &\quad \left.-\frac{1}{N^2}\left\langle\left\langle\sum_{m,n=1}^{N}\mathbf{\Phi}_{mn}\right\rangle\right\rangle\cdot\left\langle\left\langle\sum_{k,l=1}^{N}\mathbf{\Phi}_{kl}\right\rangle\right\rangle\right], \\ C_{\parallel}(i) &= \frac{1}{3\sigma_0^2N^2}\left[\left\langle\left\langle\sum_{m,n=1}^{N}\mathbf{\Phi}_{mn}\cdot\mathbf{\Phi}_{m,n+i}\right\rangle\right\rangle\right. \\ &\quad \left.-\frac{1}{N^2}\left\langle\left\langle\sum_{m,n=1}^{N}\mathbf{\Phi}_{mn}\right\rangle\right\rangle\cdot\left\langle\left\langle\sum_{k,l=1}^{N}\mathbf{\Phi}_{kl}\right\rangle\right\rangle\right],\end{aligned} \tag{29}$$

with transverse coherence lengths $R_{\perp}$ and longitudinal (dimensionless) coherence rapidity $R_{\parallel}$ defined through

$$C(i)<\frac{1}{e} \quad \text{for} \quad i>\frac{R_{\perp}}{a} \quad \text{or} \quad i>\frac{R_{\parallel}}{b}, \tag{30}$$

respectively. For the initial ensemble (22) the correlations are, of course, isotropic on the lattice, i.e.

$$\frac{R_{\perp}}{a}=\frac{R_{\parallel}}{b}=\frac{R_0}{a} \tag{31}$$

with initial spatial coherence length R_0. In the continuum limit ($a\to0$, $N\to\infty$), we obtain $C(r)$ as function of the spatial distance r [or rapidity $\eta=r(b/a)$]

$$C(r) = \frac{e^{-(m/\mathcal{T})(\sqrt{1+r^2\mathcal{T}^2}-1)}}{(1+r^2\mathcal{T}^2)^{3/2}}\left(\frac{1+(m/\mathcal{T})\sqrt{1+r^2\mathcal{T}^2}}{1+m/\mathcal{T}}\right). \tag{32}$$

Specifically, putting $m=0$, the coherence length R as defined in (30) is

$$R = \frac{\sqrt{e^{2/3}-1}}{\mathcal{T}} \approx \frac{0.97}{\mathcal{T}}. \tag{33}$$

This allows us to put limits on the range of temperatures that can be reasonably represented on the lattice. Typically, for lattice size of $N\sim100$, $\mathcal{T}$ should lie within the range from

about 0.02 to about 0.8 inverse lattice units. For smaller values the initial coherence length already covers more than half of the lattice so almost no defects will fit on the lattice, for larger values the correlation lengths approach the lattice constant. It may be noted that with (24), for $(\ell/a)\sim 5$ and $(a\mathcal{T})\sim 0.1$, the ratio $m/\mathcal{T}$ is not very small, so generally we expect appreciable deviations from the $\mathcal{T}^{-1}$ scaling in (33) [e.g., for $(\ell/a)=4$ we find $(R/a)\sim(a\mathcal{T})^{-0.8}$ (cf. Fig. 3)].

During the evolution in the Bjorken frame the correlations rapidly become anisotropic. We then conveniently define an average coherence length $\overline{R}$ through

$$\frac{a^2}{\overline{R}^2}=\frac{1}{2}\left(\frac{a^2}{R_\perp^2}+\frac{b^2}{R_\parallel^2}\right). \tag{34}$$

This may be compared to the coherence radius obtained from the angular-averaged correlation function

$$\overline{C}(r)=\frac{1}{3\sigma_0^2N^2}\left[\left\langle\left\langle\sum_{m,n=1}^{N}\sum_{i,j}\mathbf{\Phi}_{mn}\cdot\mathbf{\Phi}_{m+i,n+j}\right\rangle\right\rangle-\frac{1}{N^2}\left\langle\left\langle\sum_{m,n=1}^{N}\mathbf{\Phi}_{mn}\right\rangle\right\rangle\cdot\left\langle\left\langle\sum_{k,l=1}^{N}\mathbf{\Phi}_{kl}\right\rangle\right\rangle\right], \tag{35}$$

where the i,j sum indicates an average over all lattice points in a narrow circular ring with radius r around the lattice point mn.

The essential characteristics of the evolutions are not very sensitive to the choice of the initial time derivatives. (They can as well be put to zero.) The equations of motion very quickly establish appropriate velocities. Of course, the absolute value of the total energy depends on that choice. For the simulations presented in the following we construct in analogy to the initial configurations (18) an initial ensemble of time derivatives through

$$(\partial_\tau\mathbf{\Phi})_{ij}=\frac{\mathrm{i}}{N}\sum_{k,l=-N/2+1}^{N/2}\frac{\omega_{kl}}{2}(e^{\mathrm{i}(2\pi/N)(i\cdot k+j\cdot l)}\tilde{\mathbf{\Phi}}_{kl}-\text{c.c.}),$$

with

$$\omega_{kl}=\sqrt{\left(\frac{2\pi}{aN}k\right)^2+\left(\frac{2\pi}{aN}l\right)^2+m^2}. \tag{36}$$

The Fourier coefficients $\tilde{\mathbf{\Phi}}_{kl}$ again are picked randomly from the same Gaussian deviate (22).

IV. SHRINKING SOLITONS IN COMOVING FRAMES

Let $\mathbf{\Phi}^{(s)}(x,z)$ be a static soliton solution of the model (2) in its (x,z) rest frame, which minimizes the static energy $E=L+U$ with a finite value for the soliton energy $E=E_0$. After the transformation to the Bjorken frame, the configuration $\mathbf{\Phi}_\tau^{(s)}(x,\eta)=\mathbf{\Phi}^{(s)}(x,\tau\eta)$ then describes a static solution of the action in the comoving (x,η) frame at proper time τ [where ∂_z is replaced by $(1/\tau)\partial_\eta$], for the same value

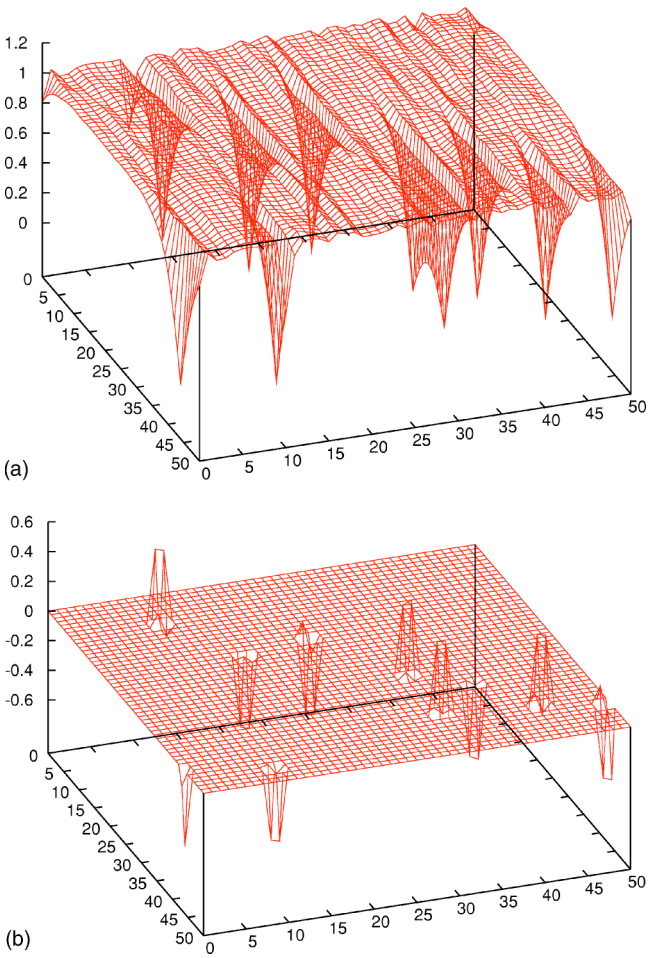

FIG. 1. (Color online) Soliton configuration after a typical evolution on a 50×50 lattice (for $\lambda=1$, $\ell/a=4$, $\sigma_0=0.2$, $H=0.2$, $a\mathcal{T}=0.2$) at time $\tau/\tau_0=1000$, i.e., long after completion of the roll-down. The bag field $|\mathbf{\Phi}|$ of the solitons (upper part) is squeezed longitudinally to lattice-unit size; the positive or negative winding densities (lower part) are located at the center of the bags.

of E_0. It represents a soliton with the same finite radius in transverse x direction as before, but with its radius in longitudinal η direction shrinking like $1/\tau$ with increasing proper time τ. The total energy E_0 of this shrinking soliton is, of course, independent of τ. (Naturally, this consideration strictly applies only to the adiabatic case, where τ is considered as a parameter. In the dynamical ordering process the evolution of the solitons towards their static form may appreciably lag behind the actual progress of proper time.)

For lattice implementations, with the typical spatial radius of the stable solitons given by ℓ, the longitudinal extension of the solitons for times $\tau\gg\ell$ has shrunk down to (dimensionless rapidity) lattice-unit size and longitudinally adjacent solitons no longer interact. In the transverse direction, however, the solitons develop their stable size of ℓ/a lattice units, they keep interacting, attracting close neighbors, or annihilating with overlapping antisolitons (cf. Fig. 1).

For solitons shrinking longitudinally down to lattice-unit size the energy will begin to deviate from the value E_0 as soon as the longitudinal extent covers merely a few lattice units. To get an approximate idea for the energy limit let us

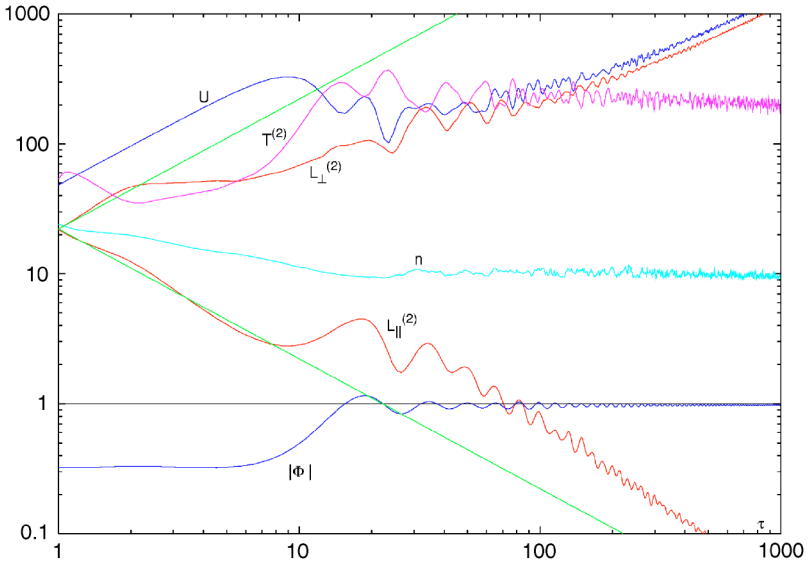

FIG. 2. (Color online) Potential energy U, kinetic energy $T^{(2)}$, transverse and longitudinal (second-order) gradient terms $L_{\perp}^{(2)}$ and $L_{\|}^{(2)}$, the number of defects n, and the average length of the chiral field $|\mathbf{\Phi}|$, for a typical evolution after a sudden quench (for $\lambda=1$, $\ell/a=4$, $\sigma_0=0.2$, $H=0.2$, $a\mathcal{T}=0.2$, $N=50$). For comparison, the straight lines given by Eqs. (45) with (43) are included.

assume that a single separate soliton finally degenerates into a transverse string of $2\ell+1$ lattice points, on which $|\mathbf{\Phi}|$ varies from nearly zero (in its center) to the surrounding vacuum configuration $\mathbf{\Phi}_0=(0,0,1)$, i.e., $\mathbf{\Phi}=(0,0,|i|/\ell)$ for $-\ell\leqslant i\leqslant\ell$, on that string of lattice points. Then we find for the contributions of a single soliton

$$L_{\perp}^{(2)}\sim\frac{\tau}{\ell},\quad L_{\|}^{(2)}\sim\frac{\ell}{\tau},\quad U\sim\lambda\frac{\tau}{\ell}. \tag{37}$$

So, apparently, solitons shrinking on a lattice contribute to the energy terms that rise linearly with proper time τ which (as lattice artifact) will dominate the total energy for large τ.

We expect the winding density of the squeezed defect to be located on ν lattice squares near its center. This implies for the fourth-order term

$$L_{\|}^{(4)}=\frac{\lambda\ell^2/\nu}{\tau}. \tag{38}$$

The winding density is determined by the orientation of the field unit vector alone, so it is sufficient to consider the unit vectors $\hat{\mathbf{\Phi}}$. We expect the squeezed defect to consist of just one unit vector $\hat{\mathbf{\Phi}}=(0,0,-1)$ at the soliton center looking into the direction opposite to all surrounding unit vectors $(0,0,1)$. That lattice point is the top of four adjacent rectangular triangles (with the diagonals connecting the four nearest-neighbor points as bases) that together cover an area of two lattice squares. So we expect a winding density $\rho=1/\nu$ with $\nu\sim 2$.

This dominance of lattice artifacts for $\tau\gg\ell$ is illustrated in Fig. 2, which shows a typical evolution on a 50×50 lattice for $\ell=4$. The total winding number is $B=-1$. After the roll-down the number of solitons stabilizes at $n=9$ (cf. Fig. 1). Apparently, both U and $L_{\perp}^{(2)}$ approach a linearly rising limit for $\tau\gg 10^2$, approximately like $\sim\frac{1}{2}n(\tau/\ell)$, which dominates the total energy, but does not affect the (essentially constant) kinetic energy. Longitudinal contributions drop off like τ^{-1}, so they are irrelevant.

It appears from Fig. 2 that for this evolution the roll-down (where the average of Φ approaches the vacuum value $\Phi=1$) takes place during the time interval $2\ell<\tau<4\ell$, i.e., long before artificial lattice effects dominate the energy. It is also by the end of the roll-down that the number of created defects stabilizes. So we would conclude that results obtained from lattice simulations for baryon-antibaryon production during the chiral phase transition in a rapidly expanding chiral gas are not severely affected by lattice artifacts. On the other hand, to follow the evolutions beyond the end of the roll-down, which comprise small σ and π oscillations of $\mathbf{\Phi}$ around the true vacuum, interfering with small oscillations of the bag profiles (resonances), will require us to subtract the lattice artifacts.

V. EVOLUTION UNTIL FREEZE-OUT

In this chapter we will follow typical evolutions of the chiral field after a sudden quench in more detail and try to analyze their characteristic features up to the end of the roll-down. Immediately before the sudden quench at $\tau=\tau_0$ the initial ensemble is prepared as described in Sec. II. The average length of one component of the chiral field is given by σ_0 [cf. Eq. (27)], the potential in (6) is characterized by a negative value of f^2. So, for sufficiently small σ_0^2 we have at $\tau=\tau_0$

$$U_0=\tau_0\frac{\lambda}{4\ell^2}\int(f^4+2|f^2|\langle\langle\mathbf{\Phi}^2\rangle\rangle)dx\,d\eta=(C_0+C_2)\mathcal{V}_0, \tag{39}$$

where $\mathcal{V}_0=\tau_0\Delta\eta\mathcal{A}$ is the initial volume of the Bjorken slice, and the constants are

$$C_0=\frac{\lambda}{4\ell^2}f^4,\quad C_2=\frac{3\lambda}{2\ell^2}|f^2|\sigma_0^2. \tag{40}$$

For the derivatives at lattice points (i,j) Eq. (18) implies

$$(\partial_x \mathbf{\Phi})_{ij} = \frac{\mathrm{i}}{N} \sum_{k,l=-N/2+1}^{N/2} \left(\frac{2\pi k}{aN} \right) e^{\mathrm{i}(2\pi/N)(i\cdot k + j\cdot l)} \tilde{\mathbf{\Phi}}_{kl},$$

$$(\partial_\eta \mathbf{\Phi})_{ij} = \frac{\mathrm{i}}{N} \sum_{k,l=-N/2+1}^{N/2} \left(\frac{2\pi l}{bN} \right) e^{\mathrm{i}(2\pi/N)(i\cdot k + j\cdot l)} \tilde{\mathbf{\Phi}}_{kl}. \tag{41}$$

Again replacing the integrands in (13) and (14) by ensemble averages leads to the second-order gradient contribution at $\tau = \tau_0$,

$$L_0^{(2)} = C^{(2)} \mathcal{V}_0. \tag{42}$$

For the constant $C^{(2)}$ we have in the continuum limit

$$C^{(2)} = \frac{9}{2} \sigma_0^2 \mathcal{T}^2 \left(1 + \frac{m^2}{3\mathcal{T}^2 (1 + m/\mathcal{T})} \right). \tag{43}$$

Similarly, one may obtain a rough estimate for $L^{(4)}$ averaged over the initial ensemble by replacing in (5) the unit vectors $\hat{\mathbf{\Phi}}$ by $\mathbf{\Phi}/\sigma_0$.

During the very early phase of an evolution in proper time the initially random ensemble of fluctuations will essentially stay random. This means that the integrals in (13)–(15) will remain constant, given by their initial values. Therefore, the time dependence of the different contributions (13)–(15) to the total energy is given by the kinematical factors (τ/τ_0) or (τ_0/τ) alone, with the integrals approximated by replacing the integrands through their averages in the initial ensemble.

After the quench, f^2 is positive, so for sufficiently small σ_0^2 we have

$$U = \tau \frac{\lambda f^2}{4\ell^2} \int (f^2 - 2\langle\langle \mathbf{\Phi}^2 \rangle\rangle) dx d\eta = \frac{\tau}{\tau_0} (C_0 - C_2) \mathcal{V}_0 \tag{44}$$

and

$$L_\perp^{(2)} = \frac{\tau}{\tau_0} C^{(2)} \mathcal{V}_0, \quad L_\parallel^{(2)} = \frac{\tau_0}{\tau} C^{(2)} \mathcal{V}_0. \tag{45}$$

In Fig. 2 both straight lines, (45) with (43), are included for comparison. It may be observed that the integral $L_\parallel^{(2)}$ involving the longitudinal gradients follows the straight line decrease almost until the onset of the roll-down. This means that the rapidity gradients basically stay random. On the other hand, the integral $L_\perp^{(2)}$ follows the linear rise only for about one unit of proper time after the onset of the evolution. Already near $\tau/\tau_0 \sim 2$, the transverse gradients are strongly affected by the dynamics and interfere with the kinetic energy. Due to the relative factor of $1/\tau^2$ of $L_\parallel$ as compared to $L_\perp$ the dynamics quickly gets dominated by the transverse gradients alone, such that the average kinetic energy follows the average transverse-gradient energy $L_\perp^{(2)}$, while the rapidity gradients (in $L_\parallel^{(2)}$ and $L_\parallel^{(4)}$) that decrease like $1/\tau$ are no longer relevant for the overall dynamical evolution.

Disregarding rapidity gradients altogether, the EOM (17) reduces to

$$\frac{1}{\tau} \partial_\tau \mathbf{\Phi} + \partial_{\tau\tau} \mathbf{\Phi} - \partial_{xx} \mathbf{\Phi} - m^2 \mathbf{\Phi} = \mathbf{0}, \tag{46}$$

which describes wave propagation in transverse direction, $A(\tau)\exp(ipx)$. Here the mass m^2 again characterizes the fluctuations around $\mathbf{\Phi} = \mathbf{0}$,

$$m^2 = \lambda f^2/\ell^2, \tag{47}$$

so m^2 is negative for negative f^2 (where $\mathbf{\Phi} = \mathbf{0}$ is the stable minimum), and it is positive for potentials that actually do have a lower symmetry-breaking minimum. The amplitudes $A(\tau)$ generically are Bessel functions,

$$A(\tau) \sim J_0(\tau\sqrt{p^2 - m^2}) \quad \text{for} \quad p^2 - m^2 > 0,$$

$$A(\tau) \sim I_0(\tau\sqrt{m^2 - p^2}) \quad \text{for} \quad p^2 - m^2 < 0. \tag{48}$$

For large values of their arguments the amplitudes of J_0 decrease like $1/\sqrt{\tau}$, while I_0 contains exponentially rising parts. Modes with large transverse wave numbers contribute most to $L_\perp^{(2)}$. Therefore, with their amplitudes decreasing like $1/\sqrt{\tau}$, the kinematical factor τ in $L_\perp^{(2)}$ is compensated. So we expect that the linear rise of $L_\perp^{(2)}$ ends as soon as the dynamics is dominated by the transverse gradients and is followed by a phase where

$$\langle\langle T \rangle\rangle \sim \langle\langle L_\perp^{(2)} \rangle\rangle \sim \text{const}|_\tau. \tag{49}$$

For negative m^2 no amplification occurs. After the quench, however, when f^2 has become positive, a few modes with small transverse wave numbers will start to get amplified. Typically, for wave numbers $p = 2\pi k/N$, with k integer $(0 \leqslant k \leqslant N/2)$, waves with $k/N < \sqrt{\lambda} f/(2\pi\ell)$ get amplified, e.g., the lowest three or four out of $N = 100$ for $\ell \sim 5$ (for $\lambda = 1$ and $f^2 = 1$). At first, the rate of amplification is slow because the exponential rise is compensated by a decreasing function for small arguments in $I_0(x)$. These low-k modes do not contribute much to $L_\perp^{(2)}$. In fact, the $k = 0$ mode, which experiences the largest rate of amplification, does not contribute at all.

While the amplification effect is not very pronounced for $L_\perp^{(2)}$, the few slowly exponentially rising contributions from the lowest-momentum transverse waves cause a noticeable rise of the condensate $\langle\langle \Phi^2 \rangle\rangle$ after some time. This enters into the fluctuating part C_2 of the potential U and drives it away from its linear rise given by (44). Then also the fourth-order terms in the potential become important and the dynamical evolution subsequently is dominated by the local potential. This initiates the roll-down of the field configuration at the majority of the lattice points into the true vacuum $\mathbf{\Phi}_0 = (0,0,1)$. The transition into the symmetry-violating configuration takes place, with formation of bags and solitons in those regions where the winding density happens to be high.

To estimate the time τ_1 for the onset of the roll-down we consider the $k = 0$ mode with amplitude $I_0(\tau m)$. Amplification of this amplitude by a factor e in the time interval from τ_0 to τ_1 requires

$$\ln I_0(\tau_1 m) = 1 + \ln I_0(\tau_0 m). \tag{50}$$

The right-hand side (r.h.s.) depends only very weakly on τ_0, as long as $(\tau_0 m) \leqslant 1$. In fact, $(\tau_1 m)$ varies only from 2.26 to 2.55 for $0 \leqslant (\tau_0 m) \leqslant 1$. So, for convenience we simply take $(\tau_1 m) \approx 5/2$ if $(\tau_0 m)$ is of the order of 1 or less. Otherwise, for larger values of $(\tau_0 m)$, τ_1 has to be obtained more accurately from (50). Typically, therefore, the transition from the gradient-dominated to the potential-dominated phase, happens near

$$\tau_1 \sim \frac{5\ell}{2\sqrt{\lambda f^2}}. \tag{51}$$

However, up to this time τ_1 of the onset of the roll-down, i.e., throughout the whole gradient-dominated phase the potential plays no significant role. The overall evolution proceeds practically independently from the (positive or negative) value of f^2 in the Φ^4 potential (6). This also implies that the quench time (the time scale for changes in f^2) is irrelevant as long as it is smaller than the time during which the gradient terms dominate the evolution and it justifies the use of the sudden quench approximation where we impose the ''cold'' ($\mathcal{T}=0$) potential from the outset at $\tau > \tau_0$.

With $\ell/\tau_0 > 1$, the ratio $(\tau_1/\tau_0)^2$ is sufficiently large to render all longitudinal (rapidity) gradients unimportant as compared to the potential. This means that during the subsequent roll-down different rapidity slices become effectively decoupled, and begin to evolve independently from each other, while in longitudinal direction the solitons contract to lattice unit size. Within these rapidity slices, π and σ modes propagate transversely, and eventual further annihilations of soliton-antisoliton pairs take place while the transverse shapes of the squeezed bags are established.

By the end of the roll-down the remaining nontrivial and sufficiently separate structures have essentially reached their stable form. Apart from small fluctuations, the integral (or sum) over the absolute values of the winding density $n = \int |\rho| dx dz$ then stabilizes and counts the (integer) number of these defects. Therefore we identify the end-of-the-roll-down time with the (chemical) freeze-out time τ_f when the numbers of baryons and antibaryons created are fixed. A rough estimate for τ_f may be obtained if we follow the further amplification of the amplitudes $I_0(\tau m)$ of the $k=0$ modes beyond τ_1. For large arguments the increase in $I_0(\tau m)$ is mainly due to the exponential $\exp(\tau m)$, so we obtain

$$\tau_f \sim \tau_1 + \frac{\ell}{\sqrt{\lambda f^2}} \ln\left(\frac{\Phi(\tau_f)}{\Phi(\tau_1)}\right). \tag{52}$$

For a typical amplification ratio of 5 to 10 during roll-down we then find an approximate freeze-out time of

$$\tau_f \sim \frac{4\ell}{\sqrt{\lambda f^2}}. \tag{53}$$

This certainly represents a lower limit for the duration of the roll-down, because the increasing Φ^4 contributions to the potential will slow down the symmetry-breaking motion. The numerical simulations confirm this simple argument and indicate that $(m\tau_f) \sim 4-5$ provides a reasonably accurate estimate for the freeze-out time [as long as $(\tau_0 m) \leqslant 1$]. After the quench, when f_0^2 has assumed its $\mathcal{T}=0$ value $f_0^2 = 1$, we may neglect the small contributions of the explicit symmetry-breaking H to f^2 and to the σ mass m_σ^2 in Eqs. (7) and (8) and rewrite (53) in the form

$$\frac{\tau_f}{\tau_0} \approx \frac{4\sqrt{2}}{\tau_0 m_\sigma}. \tag{54}$$

The typical example for an evolution given in Fig. 2 shows how during the roll-down the configurations pick up an appreciable amount of kinetic energy until the potential starts to deviate from its linear rise and interferes with $\langle\langle T\rangle\rangle$. Subsequently, $\langle\langle U\rangle\rangle$ starts to pick up the unphysical linearly rising lattice contributions (37) of the shrinking solitons, while the time-averaged $\langle\langle T\rangle\rangle$ remains basically constant. As the heavy solitons carry no kinetic energy, $\langle\langle T\rangle\rangle$ then resides in small transversely propagating fluctuations that eventually are emitted as σ and π mesons.

A. Correlation lengths and defect numbers

In contrast to the integer net-baryon number $B = \int \rho d^2x$, the integral (or lattice sum) over the absolute values of the local winding density $|\rho|$

$$n = \int |\rho| dx dz \tag{55}$$

generally is not an integer. The ensemble average of n is closely related to the coherence length R for the field unit vectors in the statistical ensemble of O(3)-field configurations. If an O(n) field is implemented on a d-dimensional cubic lattice with lattice constant a, then the field orientations on the vertices of a sublattice with lattice unit R/a can be considered as statistically independent. Then the average $\langle\langle n\rangle\rangle$ expected on an N^d lattice is

$$\langle\langle n\rangle\rangle = \nu_d (aN/R)^d, \tag{56}$$

where ν_d is the average fraction of the surface of the sphere $\mathbf{S}^d$ covered by the image of the sublattice unit (this is the very definition of a winding density). The number ν_d can be estimated for different manifolds [17]. For the map (compactified) $\mathbf{R}^2 \to \mathbf{S}^2$ defined by the unit vectors $\hat{\mathbf{\Phi}}(x,z)$ of the O(3) field in $d=2$ dimensions it is $\nu_2 = 1/4$ (i.e., $1/2^{d+1}$ for each of two triangles that make up each square sublattice unit cell).

Inserting our result (33) (obtained for $m=0$) into this estimate for $d=2$ dimensions, leads to $\langle\langle n\rangle\rangle_{\tau=\tau_0} \propto \mathcal{T}^2$. In Fig. 3a this is compared with numbers n and coherence lengths R measured for several initial configurations on an $N \times N$ lattice for different temperatures (for $N=100$ and mass $m=0$). Evidently, the finiteness of the lattice causes a

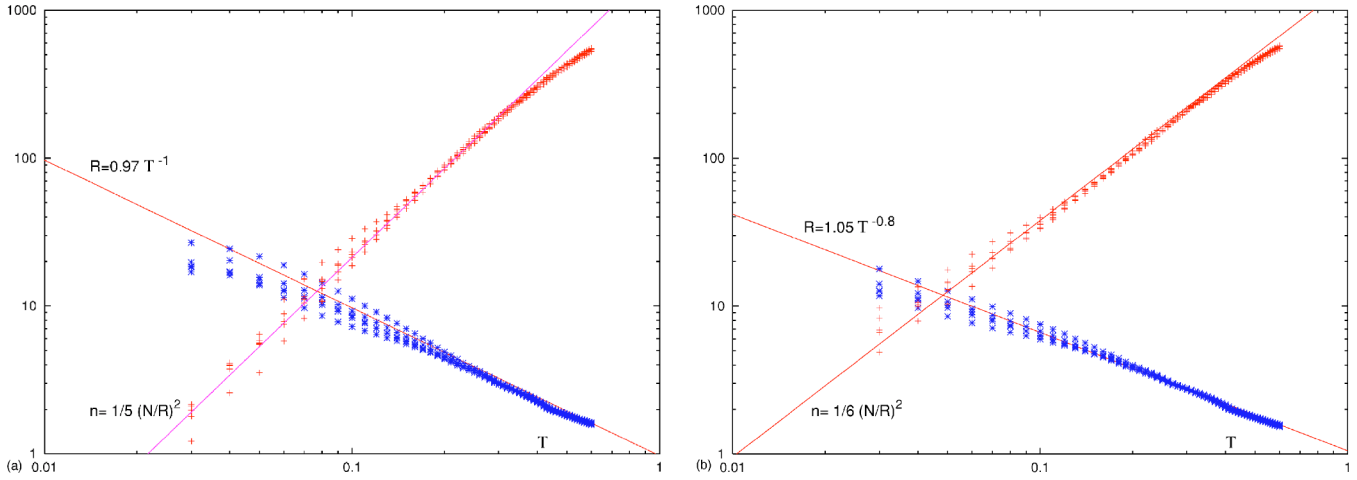

FIG. 3. (Color online) Initial (measured) coherence lengths R and number of defects n as functions of initial temperature $\mathcal{T}$, measured for five random initial configurations for each temperature, on an $N=100$ lattice, with m put to zero (left), and with $m=1/\ell$ for $\ell=4$ (right). (All quantities are in lattice units a.)

small systematic deviation from this $\mathcal{T}^2$ dependence, especially for large values of $\langle\langle n\rangle\rangle$, as the coherence length approaches the lattice constant. The measured numbers $\langle\langle n\rangle\rangle$ follow (56) with satisfactory accuracy for $\nu\approx 1/5$. In Fig. 3b the same comparison is shown for nonvanishing mass $m=1/\ell$, for $\ell/a=4$. For $m\neq 0$ the coherence length R can be obtained from (32) and compared to the measured values. Figure 3b shows that they are reasonably well described by $R\propto\mathcal{T}^{-0.8}$. The corresponding measured numbers n follow (56) with good accuracy for $\nu\approx 1/6$. Of course, small changes of ν could be absorbed into a slightly redefined coherence length [note that the correlation function (32) for $m=0$ does not decrease exponentially]. We shall, however, keep the definition (30).

The above considerations apply to random configurations that need not contain any fully developed solitons but may consist of only small fluctuating local winding densities that cover small fractions of the image sphere. However, if the configurations finally have evolved into an ensemble of well-separated solitons or antisolitons embedded in a topologically trivial vacuum with only small fluctuations in the local winding density, then the integral (55) counts the number of these embedded baryons plus antibaryons. We therefore adopt the notion ''number of defects'' for $\langle\langle n\rangle\rangle$, irrespective of whether configurations comprise only small local winding densities, or partial or complete solitons.

For a typical evolution (see e.g. Fig. 2) the number of defects measured as function of proper time shows a slow decrease that follows approximately a power law

$$n\sim n_{(\tau=\tau_0)}\left(\frac{\tau}{\tau_0}\right)^{-\gamma}. \tag{57}$$

By the end of the roll-down at freeze-out time τ_f this decrease levels off and n settles near the constant that counts the number of the finally surviving fully developed solitons plus antisolitons (cf. Fig. 1). The decrease in n reflects the slow increase in the average coherence length $\bar{R}$ up till the end of the roll-down. The longitudinal coherence length $R_\parallel$ grows very slowly because rapidity gradients are suppressed with $1/\tau$ in the Bjorken frame. This leads to an effective decoupling of field vectors in the longitudinal direction and subdues the drive for aligning field orientations in adjacent rapidity bins. On the other hand, the transverse coherence length $R_\perp$ grows rapidly. For $R_\perp \gg R_\parallel$, the average radius $\bar{R}$ obtained from (34) is dominated by $R_\parallel$. A typical example is shown in Fig. 4 for an evolution that starts at $\tau_0/a=1$. The average $\bar{R}$ grows with an exponent of $\alpha\approx 0.25$. The statistical argument in (56) then leads to $n\sim\tau^{-2\alpha}$, with $2\alpha=\gamma\approx 0.5$. This is slightly steeper than the measured decrease in n. But as the growth in the coherence radii sets in only after one or two units of τ after the onset of the evolution, the final number of surviving defects is reasonably well reproduced by the statistical expression (56) (we adopt $\nu=1/6$ from Fig. 3b). Altogether, we typically find exponents $\gamma\sim 0.4\pm 0.05$ for the decrease (57) of the number of defects. Then, with (54) for the typical freeze-out time, we have

$$\langle\langle n\rangle\rangle|_{\tau=\tau_f}=\langle\langle n\rangle\rangle|_{\tau=\tau_0}\left(\frac{\tau_0 m_\sigma}{4\sqrt{2}}\right)^{0.4} \tag{58}$$

for the reduction of the number of defects from its initial value at the onset of the evolution until the end of the roll-down. With $(\tau_0 m_\sigma)$ of the order of 0.5 to 1, we find reduction factors of 1/3 to 1/2, which is not even one order of magnitude. So, this is not a dramatic result. The reason is, evidently, that in the expanding Bjorken frame the gradient coupling in rapidity direction quickly gets suppressed.

It should be noted that all numerically measured exponents are independent of the choice of the lattice constants, because scaling $x\to ax$ (i.e., $\ell\to a\ell$), $\eta\to b\eta$, $\tau\to(a/b)\tau$ leaves the EOM (17) invariant. The length unit a only serves to define the resolution with which the spatial structure of the field configurations is analyzed and all physical results should be independent of this scale. On the other hand, the initial time τ_0 denotes the physical point in time when the

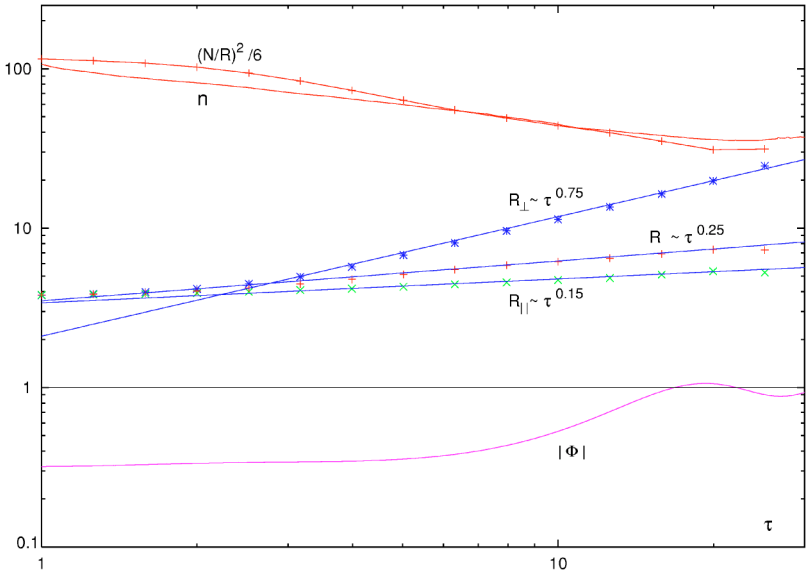

FIG. 4. (Color online) Crosses show the measured coherence lengths $R_\perp, R_\parallel$ and the average $\overline{R}$ as obtained from the definition (34), as functions of proper time τ. For $\tau > 2$ they are parametrized by power laws with exponents 0.15, 0.75, and 0.25, respectively. The measured defect number n (full line) is compared to the statistical result (56) with $\nu = 1/6$ (crosses connected by lines). ($N = 100$, $\mathcal{T} = 0.2$, $\sigma_0 = 0.2$, $\ell = 4$, $H = 0.1$, $\lambda = 1$).

system begins its evolution in terms of hadronic degrees of freedom with a sudden or rapid quench in the relevant potential. So, physical results generally will depend on τ_0, as is evident from the reduction factor obtained in (58).

Small explicit symmetry breaking ($H \neq 0$) accelerates the decrease of n during roll-down, but at the same time it reduces the freeze-out time, such that the final number of n remains essentially unaffected by small nonzero values of H. Figure 5 shows a number of evolutions for two different strengths H of explicit symmetry breaking.

The same is true if additional damping is introduced into the EOM (17) by adding a term $\kappa \partial_\tau \mathbf{\Phi}$ with damping constant κ to account for the fact that the field fluctuations are actually emitted from the expanding Bjorken rod, carrying away energy. Through this dissipative dynamics the evolutions are slowed down, the roll-down times may be retarded by an order of magnitude, but the overall reduction factor in the number of surviving defects remains unaffected. Of course, all fluctuations then are damped away during the course of the evolution, and the integrals (13) to (15) finally are determined by the remaining ensemble of squeezed solitons alone, while the kinetic energy goes to zero.

B. Meson spectrum

For times long after the roll-down the average kinetic energy $\langle\langle T \rangle\rangle$ and the potential energy parts $\langle\langle L_\perp + U \rangle\rangle$ [after subtraction of the linearly rising (lattice) contributions from the squeezed solitons (37)] converge towards the same constant $E_f/2$. Their sum E_f represents the average total energy stored in the mesonic field fluctuations after the roll-down. Both averages show residual fluctuations around their smooth background with opposite phases, such that their sum E_f is smooth. Analyzing the spectral density of either $\langle\langle T \rangle\rangle$ or $\langle\langle L_\perp + U \rangle\rangle$ (after subtracting the background), tells us about the spectral distribution of pions and σ mesons that will eventually be emitted from the expanding Bjorken rod.

We consider the Fourier transforms

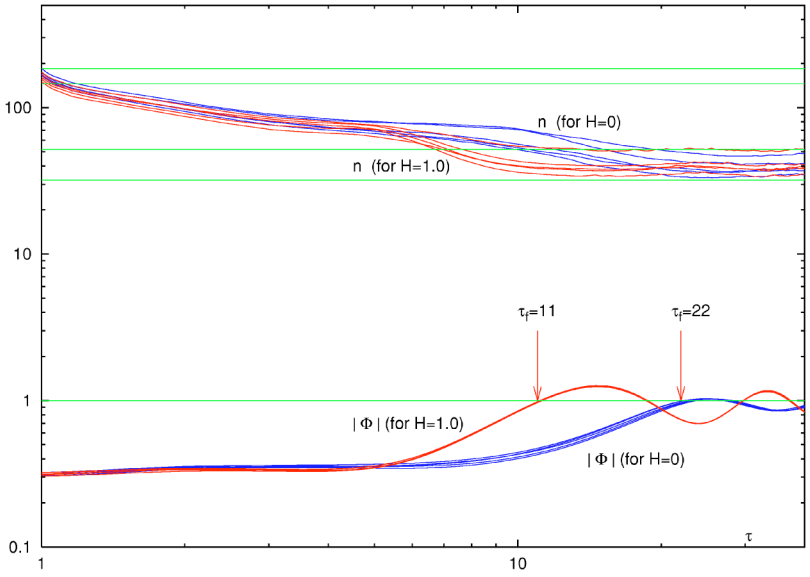

FIG. 5. (Color online) The numbers of defects n for two different values $H = 0$ and $H = 1.0$ for the strength of the explicit symmetry breaking, each for five evolutions on a 100×100 lattice ($\mathcal{T} = 0.3$, $\lambda = 1$, $\ell = 5$, $\sigma_0 = 0.2$). The arrows point to the freeze-out times $\tau_f \approx 22$, and $\tau_f \approx 11$, respectively, where the average lengths $|\mathbf{\Phi}|$ of the chiral field vectors have reached $|\mathbf{\Phi}| = 1$. The initial values of n lie within a band from 145 to 185, and they all end (for both values of H) in a band from 32 to 52, which corresponds to reduction factors of about 1/4.

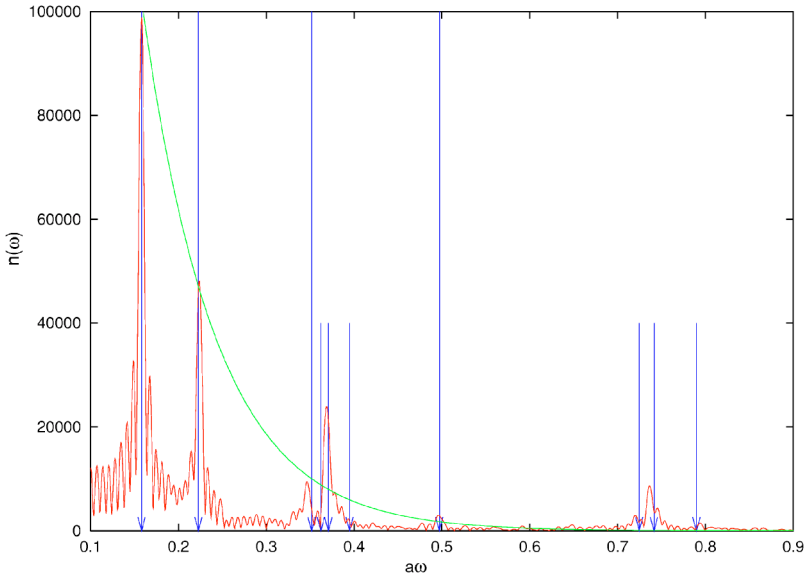

FIG. 6. (Color online) Spectral density $n(\omega)$ of the residual fluctuations in the average kinetic energy $\langle\langle T\rangle\rangle$ for times long after the roll-down ($N=80$, $\ell/a=4$, $H=0.1$). The arrows point to the lowest (double) frequencies (61) for π and σ mesons (see text). The curved (green) line is the exponential $\exp(-12a\omega)$.

$$c(\omega)+is(\omega)=\int_{\tau_a}^{\tau_b}\langle\langle T(\tau)-\overline{T}(\tau)\rangle\rangle e^{i\omega\tau}d\tau, \tag{59}$$

where the integral covers times long after the roll-down, e.g., $\tau_a/\tau_0\sim 100$, $\tau_b/\tau_0\sim 1000$, and $\overline{T}(\tau)$ subtracts the smooth background. The absolute value, $\epsilon(\omega)=\sqrt{c^2+s^2}$, represents a spectral energy density, from which we may extract the spectral particle number density

$$n(\omega)=\frac{\epsilon(\omega)}{\omega}=\sum_{ij} n_{ij}^{(\pi)}\delta(\omega-2\omega_{ij}^{(\pi)})+\sum_{ij} n_{ij}^{(\sigma)}\delta(\omega-2\omega_{ij}^{(\sigma)})+\cdots. \tag{60}$$

The ij sum with $i,j=0,1,2,\ldots,N/2$ covers all frequencies on the lattice for pions and σ mesons with masses m_π and m_σ given in (8)

$$\omega_{ij}^{(\pi/\sigma)}=\sqrt{\left(\frac{2\pi}{aN}i\right)^2+\left(\frac{2\pi}{aN}j\right)^2+m_{\pi/\sigma}^2}. \tag{61}$$

Generically, $T(\tau)$ contains contributions $\sim[\cos(\omega_{ij}^{(\pi)}\tau)]^2$ from the pionic fluctuations, and $\sim[\cos(\omega_{ij}^{(\sigma)}\tau)+c]^2$ from the σ fluctuations around some nonvanishing average c. Therefore, the spectral functions $\epsilon(\omega)$ and $n(\omega)$ will, in addition to the double frequencies $2\omega_{ij}^{(\sigma)}$, also contain contributions for the σ mesons at the single frequencies $\omega_{ij}^{(\sigma)}$.

Figure 6 shows the spectral density $n(\omega)$ as obtained from the residual fluctuations in the average kinetic energy. The long vertical arrows point to the first four $2\omega_{ij}^{(\pi)}$ pionic frequencies (61) for $ij=00,10,20,30$, with $m_\pi^2=H/\ell^2$, ($H=0.1$, $\ell/a=4$, $f_0=1$). It may be seen that the overwhelming part of the strength resides in the lowest and first excited pionic modes. The strength decreases rapidly with excitation energy, approximately like $\exp(-12a\omega)$. The same is true for the strength of the σ modes. [The short arrows in Fig. 6 point to the first three modes with $ij=00,10,20$, with single frequencies $\omega_{ij}^{(\sigma)}$ and double frequencies $2\omega_{ij}^{(\sigma)}$.] However, the number density $\Sigma n_{ij}^{(\sigma)}$ for the σ mesons, which we may extract from the strength located at the double frequencies $2\omega_{ij}^{(\sigma)}$, is only about 5% of the pionic strength residing in the first three pionic modes. For an order-of-magnitude estimate of the pionic multiplicities we therefore ignore the σ contributions.

C. Meson and baryon multiplicities

To obtain a simple estimate for the energy E_f finally available for meson production we consider the time of the onset of the roll-down τ_1 in (51), which marks the transition from the gradient-dominated to the potential-dominated phase. At this time, for sufficiently small σ_0^2, the total energy is dominated by the linearly rising term $(\tau/\tau_0)C_0\mathcal{V}_0$ in the potential (44). With the onset of the roll-down the average potential $\langle\langle U\rangle\rangle$ starts to deviate from this linear rise and bends down to interfere with $\langle\langle T\rangle\rangle$ and $\langle\langle L\rangle\rangle$ (cf. Fig. 2). In the numerical simulations the large-time limit of $\langle\langle U\rangle\rangle$ and $\langle\langle L\rangle\rangle$ is masked by the (lattice-artificial) rise of the soliton contributions. But the asymptotic $\langle\langle T\rangle\rangle$ is free of these artifacts and (apart from residual fluctuations) approaches a constant value, which is well represented by the linearly rising $\frac{1}{2}(\tau/\tau_0)C_0\mathcal{V}_0$ taken at $\tau=\tau_1$. Approximating τ_1 by $5/(\sqrt{2}m_\sigma)$ as given in (51), we then have (with $f^2=1$)

$$E_f=f_\pi^2\frac{\tau_1}{\tau_0}C_0\mathcal{V}_0\approx f_\pi^2\frac{5m_\sigma}{8\sqrt{2}}(abN^2), \tag{62}$$

where we have again neglected the small contribution of the explicit symmetry-breaking H to the σ mass. Within this level of accuracy we can also ignore that about 30% of the pions carry the energy $\omega_{10}^{(\pi)}$ (instead of m_π), and obtain the pion multiplicity n_π from dividing (62) by m_π,

$$n_\pi=\frac{5}{8\sqrt{2}}\frac{m_\sigma}{m_\pi}f_\pi^2(abN^2). \tag{63}$$

This number may be compared with the baryon-plus-antibaryon multiplicity given in (58). We use for $\langle\langle n\rangle\rangle|_{\tau=\tau_0}$ the statistical result (56), with initial spatial coherence length R_0. Then we have

$$\langle\langle n\rangle\rangle = \nu\left(\frac{aN}{R_0}\right)^2\left(\frac{\tau_0 m_\sigma}{4\sqrt{2}}\right)^\gamma. \tag{64}$$

The last factor relies on the estimates (51) and (53) for the times τ_1 and τ_f, which are valid as long as $(\tau_0 m)\leqslant 1$ [otherwise they have to be obtained more accurately from (50) and (52)]. The evolutions described above have been performed for initial configurations selected with net baryon number $B=0$. So, the average number n_p^- of antibaryons created during the phase transition is $\langle\langle n\rangle\rangle/2$. With typical values $\nu\sim 1/4$, $\gamma\sim 0.4$ we find for the multiplicity ratio of antibaryons to pions

$$n_p^-/n_\pi \approx 0.14\frac{a}{b}\frac{m_\pi}{m_\sigma f_\pi^2}\frac{(\tau_0 m_\sigma)^\gamma}{R_0^2}. \tag{65}$$

With an overall energy scale f_π^2 of the order of the pion mass m_π, and R_0 of the order of $m^{-1}=\sqrt{2}m_\sigma^{-1}$, this ratio is

$$n_p^-/n_\pi \approx 0.07\left(\frac{a}{b}m_\sigma\right)(\tau_0 m_\sigma)^\gamma. \tag{66}$$

The ratio a/b of the spatial and rapidity lattice constants which appears in this result has a physical meaning: according to (31) it is equal to the ratio of the (transverse) spatial coherence length R_0 and the (longitudinal) rapidity coherence distance $R_{\|0}$ in the initial configuration. Naturally, this ratio is of the order of τ_0. So, for initial times τ_0 typically of the order of the inverse σ mass we find antibaryon-to-pion multiplicity ratios of the order of 0.05 to 0.1.

VI. GENERALIZATION TO 3D O(4)

For the generalization to the (3+1)-dimensional O(4) model we keep the parametrization as given in Eqs. (2), (3), and (6). In this case f_π^2 is an overall constant of dimension [mass^2], so the physical fields $f_\pi\mathbf{\Phi}$ are of mass-dimension one. The winding density is no longer given by (4), but we keep $\mathcal{L}^{(4)}$ as defined by the second equality in Eq. (5). Conventionally, the strength of the $\mathcal{L}^{(4)}$ term in (5) is given in terms of the Skyrme parameter e as

$$\frac{2\lambda\ell^2}{(8\pi)^2} \Rightarrow \frac{1}{4e^2 f_\pi^2}. \tag{67}$$

In this case the typical spatial radius of a stable skyrmion in its rest frame is mainly determined by the balance between $\mathcal{L}^{(2)}$ and $\mathcal{L}^{(4)}$, so it is of the order of $(ef_\pi)^{-1}$.

For the map (compactified) $\mathbf{R}^3\to\mathbf{S}^3$ defined by the unit vectors of the O(4) field in 3 spatial dimensions the statistical result (56) for the average number of defects found on a $(aN)^3$ lattice for initial configurations with coherence length R_0 generalizes as

$$\langle\langle n\rangle\rangle|_{\tau=\tau_0} = \frac{5}{2^{3+1}}(aN/R_0)^3. \tag{68}$$

(We again use $a=b\tau_0$ for the lattice constants.) The factor 5 counts the number of three-simplices (tetraeders) that make up a cubic sublattice cell of size R_0^3, the factor $(1/2^{d+1})$ with $d=3$ is the (absolute value of the) average surface area covered by the image of one three-simplex on the image sphere $\mathbf{S}^3$. So the factor 5/16 counts the average ''number of defects'' associated with a cubic lattice cell with lattice constant given by the initial coherence length R_0. A certain arbitrariness in the definition of the coherence length may translate into modifications of this factor 5/16 [e.g., for a random lattice of three-simplices the factor 5 is replaced by $(24\pi^2/35\sim 6.8)$ [17]]. In any case we do not expect order-of-magnitude changes in this factor as compared to the $d=2$ case, where we had $2/2^{2+1}$.

However, through the cubic power the result is now very sensitive to the actual value of R_0 in the initial ensemble. Different concepts about the physical nature of the initial configurations will imply quite different ways to arrive at the appropriate initial coherence lengths R_0. For an initial ensemble that is characterized by a temperature $\mathcal{T}$ we could proceed as in (32) and relate R_0 to the temperature, or to the mass $m^2(\mathcal{T})=\lambda|f^2(\mathcal{T})|/\ell^2$ of the field fluctuations; but it has also been suggested [22] to tie R_0 to the parton density, which makes it independent of the temperature concept. So, for the moment it seems appropriate to keep the initial coherence length R_0 as a parameter.

Adding a second transverse dimension does not change the result (34) for the average of the transverse and longitudinal coherence lengths. The growth in the resulting $\overline{R}$ again is dominated by the slow increase of the longitudinal coherence length $R_\|$, which is unaffected by additional transverse dimensions. The estimates (51) and (53) for the times τ_1 and τ_f of the onset and end of the roll-down also remain unaffected, as they only rely on the amplitudes $A(\tau)$ of the transverse waves (48), irrespective of the number of spatial dimensions. [In this case, $\mathcal{L}^{(4)}$ now contributes to $L_\perp$ with a term containing four transverse gradients, acting on the direction of the O(4) field. The roll-down, however, takes place in areas that are topologically trivial, i.e., with small angular gradients, so we do not expect a strong effect on the roll-down times.] Within the approximations that led to (58), we then find for the average number of baryons and antibaryons present after the roll-down

$$\langle\langle n\rangle\rangle_{|\tau=\tau_f} = \frac{5}{16}\left(\frac{aN}{R_0}\right)^3\left(\frac{\tau_0 m_\sigma}{4\sqrt{2}}\right)^{3\alpha}, \tag{69}$$

with $\alpha\sim 0.2$ to 0.25. We denote the transverse area $(aN)^2$ of the Bjorken rod by $\mathcal{A}$, and replace the ratio (a/b) of the lattice constants again by the initial time τ_0. Then we obtain for the rapidity density of antiprotons $(n_p^-=\frac{1}{4}\langle\langle n\rangle\rangle)$

$$\frac{dn_p^-}{d\eta} = \frac{5}{64}\frac{\tau_0\mathcal{A}}{R_0^3}\left(\frac{\tau_0 m_\sigma}{4\sqrt{2}}\right)^{3\alpha} \tag{70}$$

(at this point we count all baryons as nucleons, assuming that excitational fluctuations and rotations contribute to the surrounding pionic fluctuations). Although the strength of the Skyrme term does not appear explicitly in (70), the presence of the $\mathcal{L}^{(4)}$ term is essential for the formation of the solitons, because during the evolution it transforms the sum over the absolute values of average winding densities into the average number of fully developed solitons and antisolitons. So it is hidden in the growth law characterized by α.

For meson production we adopt the considerations that led to the estimate (62). Counting again all mesons as zero momentum pions we have

$$n_\pi = \frac{E_f}{m_\pi} = \frac{f_\pi^2}{m_\pi}\frac{\tau_1}{\tau_0} C_0 \mathcal{V}_0 = f_\pi^2 \frac{5}{8\sqrt{2}}\frac{m_\sigma}{m_\pi}(\mathcal{A}bN). \tag{71}$$

The rapidity density of negatively charged pions $n_{\pi^-} = \frac{1}{3} n_\pi$ then is

$$\frac{dn_{\pi^-}}{d\eta} = f_\pi^2 \frac{5}{24\sqrt{2}}\frac{m_\sigma}{m_\pi}\mathcal{A}. \tag{72}$$

In a heavy-ion collision the transverse area $\mathcal{A}$ of the Bjorken rod will correspond to the spatial overlap of the colliding relativistic nuclear slabs. As we have assumed spatially homogeneous initial conditions we have to consider slabs with constant nucleon (area) density. In order to account for the number A of nucleons contained in one slab, its radius must be taken as $r_0 A^{1/2}$, with $r_0 \approx 1.2$ fm. Then, as function of centrality, $dn_{\pi^-}/d\eta$ is directly proportional to the number of participants N_p, which is one of the basic experimental results in relativistic heavy-ion collisions. For central collisions of A-nucleon slabs we have $N_p = 2A$, so we find for the π^--rapidity density per $N_p/2$ participants

$$\frac{1}{N_p/2}\frac{dn_{\pi^-}}{d\eta} = \frac{5\pi}{24\sqrt{2}}\frac{m_\sigma}{m_\pi}(r_0 f_\pi)^2. \tag{73}$$

This is an interesting result because all parameters have been absorbed into physical quantities. There are, however, several caveats: We have used for this result the form of the potential (6) *after* the quench (only this enters into the calculations). This means that differences between the average potential energy *before* the quench (39) and immediately *after* the quench (44) are left out. However, this difference is of the order σ_0^2, which has been neglected in (73) anyway. But generally, the result (73) should be considered as a lower limit. It should further be noted that the result (73) depends linearly on the time τ_1 for the onset of the roll-down. The definition of τ_1 in (51) is not very stringent and may be subject to changes by $\pm 20\%$. The estimate [cf. Eq. (51)] we used for the time τ_1 required $(\tau_0 m_\sigma) \leqslant \sqrt{2}$, i.e. with $m_\sigma \sim 3$–5 fm^{-1}, the initial time τ_0 should not exceed 0.3–0.5 fm. Another unsatisfactory feature of the homogeneous Bjorken rod is that the inhomogeneity in the nucleon (area) density of real relativistic nuclear slabs with transverse radii $r_0 A^{1/3}$ has to be represented through radii $r_0 A^{1/2}$ for homogeneous slabs.

The experimental value [16] for the π^- rapidity density per $N_p/2$ lies between 1.2 and 1.5 for N_p increasing up to 350. With $r_0 f_\pi = 0.57$, $m_\sigma/m_\pi \approx 5$–8, our result (73) leads to

$$\frac{1}{N_p/2}\frac{dn_{\pi^-}}{d\eta} \approx 0.75\text{–}1.2. \tag{74}$$

In the light of the reservations discussed above, this is quite satisfactory.

In contrast to the parameter-free pion multiplicities, the result for baryon-antibaryon creation depends on two parameters: the time τ_0 when the initial hadronic field ensemble is established and begins its expansion, and the initial coherence length R_0 within that ensemble. From (70) and (72) we have (with $\alpha \sim 0.2$ to 0.25)

$$\frac{n_p^-}{n_{\pi^-}} \approx 0.15\left(\frac{m_\pi m_\sigma}{f_\pi^2}\right)\frac{(\tau_0 m_\sigma)^{3\alpha+1}}{(R_0 m_\sigma)^3}. \tag{75}$$

The experimental value for the ratio of integrated $\bar{p}$ to π^- multiplicities lies between 0.065 and 0.085 [16] for varying numbers of participants. With $m_\pi/f_\pi^2 = 3.0$ fm, and a typical σ mass of $m_\sigma \approx 3$ fm^{-1}, the experimentally observed multiplicity ratios are reproduced if R_0 and τ_0 (both in [fm]) satisfy

$$R_0 \approx (3\tau_0)^{\alpha+1/3}. \tag{76}$$

For initial times in the range $0.2 \leqslant \tau_0 \leqslant 0.5$ the dependence on α is very weak and the coherence length varies in the range $0.7 \leqslant R_0 \leqslant 1.2$ (all in [fm]). These values are certainly within the limits of conventional assumptions. Interpreted in terms of a thermodynamic equilibrium ensemble, $R_0 \sim 1$ fm$\sim \mathcal{T}^{-1}$ implies the standard estimate $\mathcal{T} \sim 200$ MeV for the chiral phase transition. With our choice $a/b = \tau_0 = R_0/R_{\|0}$ for the ratio of the spatial and rapidity lattice constants, the initial time $\tau_0 \approx 1/3$ fm resulting from (76) for $R_0 = 1$ fm then means that in the initial ensemble the initial rapidity coherence distance $R_{\|0}$ extends over three units of rapidity.

VII. CONCLUSION

We have presented numerical simulations of the dynamical evolution that chiral field configurations undergo in a rapidly expanding spatial volume. Starting at an initial time τ_0 from a random hadronic field ensemble with restored chiral symmetry, we follow its ordering process and roll-down into the global potential minimum with spontaneously broken chiral symmetry. In accordance with standard concepts of heavy-ion physics we have considered one-dimensional longitudinal expansion of an essentially baryon-free region of high energy density, as it may be realized in the aftermath of an ultrarelativistic collision of heavy ions for central rapidities.

Performed on a space-rapidity lattice in proper time of comoving frames, such simulations are very powerful instruments that allow us to investigate a multitude of interesting features related to the chiral phase transition. We have con-

centrated here on the topological aspects that are directly related to baryon-antibaryon multiplicity as a sensitive signal for the phase transition. Mesonic abundancies could be analyzed as well, both for π and σ mesons (or any other elementary fluctuations included in the chiral field). Not only their spectra can be obtained, but from the instantaneous configurations the spectral power of their momentum distribution could be extracted at every point in time.

The method is not restricted to thermally equilibrated initial ensembles with global or local temperature; inhomogenities and anisotropy in the correlation lengths could be implemented naturally. Surface effects could be investigated by suitable boundary conditions. This may be interesting with respect to the A dependence of spectra and multiplicities. Here we have applied only standard periodic conditions. The one-dimensional expansion could be replaced by anisotropic or spherically symmetric expansion, which may be of specific interest in cosmological applications. We have used the sudden quench approximation, which could be replaced by any desired time dependence of the chiral potential with arbitrary quench times. We have selected ensembles with conserved net-baryon number $B=0$ or very small B. Any other choice would be possible, and it appears as a peculiarly attractive feature to study evolutions in ensembles with high net-baryon density, either fixed or in the form of grand canonical ensembles. The method is well suited to analyze distribution, growth, and realigning of domains with disoriented chiral condensate as has been shown previously in purely dissipative dynamics [14]. The generalization to SU(3) fields appears most interesting to learn about strangeness production in terms of baryonic and kaonic abundance ratios.

Evidently, the method opens up a wide field of applications. Unfortunately, however, we know very little about the nature and characteristics of the initial ensemble that enters crucially into all physical results. So, in our present analysis of antibaryon and pion multiplicities, the experimental data do not allow us to draw definite conclusions about the validity of the topological approach, because the results depend on two initial coherence lengths, the spatial R_0 and rapidity $R_{\|0}$ (which for an isotropic initial ensemble are related by $R_0=R_{\|0}\tau_0$). We can only conclude that conventional assumptions about these quantities lead to results that are compatible with experimentally detected multiplicities. So, luckily, the mechanism is not ruled out. On the other hand, an assumption like $\tau_0=R_0$ (which would imply that the correlations have grown with the speed of light from a pointlike origin) is ruled out: it would overestimate the abundance ratio in (75) by a factor of 5.

ACKNOWLEDGMENT

The author appreciates helpful discussions with J. Klomfass, H. Walliser, and H. Weigel.

[1] T.H.R. Skyrme, Proc. R. Soc. London Ser. A **260**, 127 (1961).
[2] B. Schwesinger, Nucl. Phys. **A537**, 253 (1992); H. Weigel, Int. J. Mod. Phys. A **11**, 2419 (1996); Y.S. Oh, D.P. Min, M. Rho, and N.N. Scoccola, Nucl. Phys. **A534**, 493 (1991).
[3] M. Chemtob, Nucl. Phys. **B256**, 600 (1985); H. Walliser, Nucl. Phys. **A548**, 649 (1992); D. Diakonov, V. Petrov, and M.V. Polyakov, Z. Phys. A **359**, 305 (1997); H. Weigel, Eur. Phys. J. A **2**, 391 (1998); LEPS Collaboration, T. Nakano *et al.*, Phys. Rev. Lett. **91**, 012002 (2003).
[4] A. Hayashi, G. Eckart, G. Holzwarth, and H. Walliser, Phys. Lett. B **147B**, 5 (1984); M.P. Mattis and M.E. Peskin, Phys. Rev. D **32**, 58 (1985).
[5] M.P. Mattis and M. Karliner, Phys. Rev. D **31**, 2833 (1985); G. Eckart, A. Hayashi, and G. Holzwarth, Nucl. Phys. **A448**, 732 (1986).
[6] S. Brodsky, J. Ellis, and M. Karliner, Phys. Lett. B **206**, 309 (1988); R. Johnson, N.W. Park, J. Schechter, V. Soni, and H. Weigel, Phys. Rev. D **42**, 2998 (1990).
[7] M.K. Jones *et al.*, Phys. Rev. Lett. **84**, 1398 (2000).
[8] G. Holzwarth, Z. Phys. A **356**, 339 (1996).
[9] E. Witten, Nucl. Phys. **B223**, 422 (1983).
[10] B. Moussallam, Ann. Phys. (N.Y.) **225**, 264 (1993); F. Meier and H. Walliser, Phys. Rep. **289**, 383 (1997).
[11] A.A. Anselm, Phys. Lett. B **217**, 169 (1988); A.A. Anselm and M.G. Ryskin, *ibid.* **266**, 482 (1991); J.P. Blaizot and A. Krzywicki, Phys. Rev. D **46**, 246 (1992); **50**, 442 (1994); J.D. Bjorken, Int. J. Mod. Phys. A **7**, 4189 (1992); S. Gavin, Nucl. Phys. **A590**, 163c (1995).
[12] I.G. Bearden *et al.*, Phys. Rev. C **65**, 044903 (2002); M.M. Aggarwal *et al.*, *ibid.* **65**, 054912 (2002); T.K. Nayak *et al.*, Pramana, J. Phys. **57**, 285 (2001); T.C. Brooks *et al.*, Phys. Rev. D **61**, 032003 (2000).
[13] S. Gavin, A. Gocksch, and R.D. Pisarski, Phys. Rev. Lett. **72**, 2143 (1994).
[14] G. Holzwarth and J. Klomfass, Phys. Rev. D **66**, 045032 (2002).
[15] T.A. DeGrand, Phys. Rev. D **30**, 2001 (1984); J. Ellis, U. Heinz, and H. Kowalski, Phys. Lett. B **233**, 223 (1989); J.I. Kapusta and A.M. Srivastava, Phys. Rev. D **52**, 2977 (1995); J. Dziarmaga and M. Sadzikowski, Phys. Rev. Lett. **82**, 4192 (1999).
[16] PHENIX Collaboration, K. Adcox *et al.*, Phys. Rev. Lett. **88**, 242301 (2002).
[17] T.W.B. Kibble, J. Phys. A **9**, 1387 (1976); N.H. Christ, R. Friedberg, and T.D. Lee, Nucl. Phys. **B202**, 89 (1982).
[18] W.H. Zurek, Nature (London) **317**, 505 (1985); G.E. Volovik, *Exotic Properties of Superfluid ^3He* (World Scientific, Singapore 1992); M. Hindmarsh and T.W.B. Kibble, Rep. Prog. Phys. **58**, 477 (1995); W.H. Zurek, Phys. Rep. **276**, 177 (1996); P. Laguna and W.H. Zurek, Phys. Rev. Lett. **78**, 2519 (1997); R.H. Brandenberger, Pramana, J. Phys. **51**, 191 (1998); G.J. Stephens, Phys. Rev. D **61**, 085002 (2000).
[19] Z. Huang and X.-N. Wang, Phys. Rev. D **49**, 4335 (1994); F. Cooper, Y. Kluger, E. Mottola, and J.P. Paz, *ibid.* **51**, 2377 (1995); M.A. Lampert, J.F. Dawson, and F. Cooper, *ibid.*

54, 2213 (1996); J. Randrup, Phys. Rev. Lett. **77**, 1226 (1996); Nucl. Phys. **A616**, 531 (1997); T.C. Petersen and J. Randrup, Phys. Rev. C **61**, 024906 (2000); O. Scavenius, A. Dumitru, and A.D. Jackson, Phys. Rev. Lett. **87**, 182302 (2001).

[20] G. Holzwarth, Phys. Rev. D **68**, 016008 (2003).

[21] G. Holzwarth and J. Klomfass, Phys. Rev. D **63**, 025021 (2001).

[22] J. Ellis and H. Kowalski, Phys. Lett. B **214**, 161 (1988).